RSC Advances

PAPER

View Article Online
View Journal | View Issue

CrossMark click for updates

Cite this: *RSC Adv.*, 2017, **7**, 3680

# Molybdenum trioxide nanopaper as a dual gas sensor for detecting trimethylamine and hydrogen sulfide†

Hua-Yao Li,[a] Liang Huang,[b] Xiao-Xue Wang,[c] Chul-Soon Lee,[a] Ji-Wook Yoon,[a] Jun Zhou,[b] Xin Guo[c] and Jong-Heun Lee*[a]

Received 4th November 2016
Accepted 1st December 2016

DOI: 10.1039/c6ra26280e

www.rsc.org/advances

A free-standing, flexible, and semi-transparent $MoO_3$ nanopaper was fabricated using ultralong $MoO_3$ nanobelts (length ~ 200 μm; width 200–400 nm), and its gas-sensing characteristics were investigated. The sensor exhibited high responses (resistance ratio) of 49 to 5 parts per million (ppm) hydrogen sulfide ($H_2S$) at 250 °C and 121 to 5 ppm trimethylamine (TMA) at 325 °C with excellent gas selectivity, demonstrating its dual function for gas detection. Moreover, the sensor showed promising potential for the all-in-one detection of three representative offensive odors (TMA, $H_2S$, and $NH_3$) simply by tuning of the sensing temperature. This particular performance is attributed to the high chemical affinity of $MoO_3$ to $H_2S$ and the acid–base interaction between basic TMA/$NH_3$ and acidic $MoO_3$. The mechanism underlying the control of gas selectivity by modulating the sensor temperature was investigated by Diffuse Reflectance Infrared Fourier Transform (DRIFT) measurements.

Open Access Article. Published on 17 January 2017. Downloaded on 8/17/2025 6:59:34 PM.
This article is licensed under a Creative Commons Attribution 3.0 Unported Licence.

## Introduction

Trimethylamine (TMA) and hydrogen sulfide ($H_2S$), which are generated by the decomposition of plants and animals, are colorless, flammable, and poisonous gases with unpleasant odors that are described as "fishy" and "rotten-eggs", respectively.[1–4] Although the smell is initially pungent, it rapidly paralyzes the olfactory system, resulting in unawareness of its presence. Exposure to a certain concentration (~10 parts per million (ppm)) of either TMA or $H_2S$ can cause not only discomfort but also headaches, nausea, and irritation to the eyes and respiratory system.[5,6] TMA and $H_2S$ are trace biomarkers (sub-ppm level)—detected in human exhaled breath—of renal-system imbalance and periodontal disease, respectively.[7,8] Accordingly, the detection of sub-ppm to ppm levels of TMA and $H_2S$ is of vital importance in food quality control, environmental monitoring, and medical diagnosis.

Metal-oxide semiconductors are widely used in gas sensors to detect trace concentrations of reducing gases because of their high response, simple structure, facile integration into small devices, and cost effectiveness.[9–11] However, oxide-semiconductor gas sensors often exhibit similar gas responses to a range of different gases, which hampers the selective detection of a specific gas. Many efforts have been made to enhance the selectivity, including the modulation of the sensor temperature,[12] the loading of noble-metal catalysts,[13,14] the doping of catalytic oxides,[15,16] and control of acid–base interactions.[17,18] Although pattern recognition using an array of sensors is one solution for gas discrimination, the number of sensors should be minimized to reduce the size, cost, power consumption, and sensing circuit of devices.[19,20] From this viewpoint, the detection of multiple gases using a single sensor is the ideal approach for realizing simple and reliable gas sensors.

To date, various metal-oxide semiconductors have been investigated for the detection of TMA and $H_2S$. $TiO_2$, $WO_3$, $MoO_3$, and $LaFeO_3$ exhibit good sensing performance toward TMA,[21–25] and ZnO, $SnO_2$, $WO_3$, CuO, $MoO_3$, and $BaCoO_3$ have been used to detect $H_2S$.[26–33] Note that, molybdenum trioxide ($MoO_3$), which has abundant Lewis-acid sites, exhibits a high reactivity to both TMA and $H_2S$, probably because of its high chemical affinity to $H_2S$ and strong interaction with basic TMA.[15,24] This suggests the possibility of the simultaneous detection of ubiquitous offensive odors (TMA and $H_2S$) using a single gas sensor.

Yang *et al.*[34] fabricated a gas sensor by drop coating a slurry containing $MoO_3$ nanobelts onto a substrate and demonstrated its potential for detecting TMA. However, neither the control of the selectivity to different offensive odors such as TMA, $H_2S$, and $NH_3$ nor the detailed gas-sensing mechanism was investigated. In the present study, $MoO_3$ nanobelts with an average length of 200 μm were synthesized by a modified hydrothermal

[a]*Department of Materials Science and Engineering, Korea University, Seoul 02841, Republic of Korea. E-mail: jongheun@korea.ac.kr*

[b]*Wuhan National Laboratory for Optoelectronics, Huazhong University of Science and Technology, Wuhan 430074, P. R. China*

[c]*Laboratory of Solid State Ionics, School of Materials Science and Engineering, Huazhong University of Science and Technology, Wuhan 430074, P. R. China*

† Electronic supplementary information (ESI) available: Response and recovery curves of $MoO_3$-nanopaper gas sensor, stability of the $MoO_3$-nanopaper sensor, and Gas-sensing performance of various sensors. See DOI: 10.1039/c6ra26280e



This journal is © The Royal Society of Chemistry 2017

Open Access Article. Published on 17 January 2017. Downloaded on 8/17/2025 6:59:34 PM.
This article is licensed under a Creative Commons Attribution 3.0 Unported Licence.

method and fabricated into a free-standing, flexible, semi-transparent ultrathin paper to increase the gas accessibility and the gas-sensing reliability. The sensor using $MoO_3$ nanopapers showed the dual functionality to detect $H_2S$ at 250 °C and TMA 325 °C both with excellent selectivity. The control of the gas selectivity, the gas response, and dual gas sensing by the modulation of the sensor temperature was investigated in relation to the gas-sensing mechanism and surface-reaction analysis using Diffuse Reflectance Infrared Fourier Transform (DRIFT) spectra.

## Experimental

Ultralong $MoO_3$ nanobelts were synthesized *via* a modified hydrothermal method.[35] 2 g of molybdenum powder (Aladdin, 99.5%) to 10 mL of deionized (DI) water and 20 mL of 30 wt% $H_2O_2$ until the solution became light yellow. The solution was stirred for 30 min to react thoroughly and then transferred to a Teflon-lined stainless-steel autoclave and heated to 220 °C for 100 h. The precipitate was filtered and rinsed by DI water and ethanol several times.

Vacuum filtration was employed to fabricate $MoO_3$ nanopapers. First, 0.82 mg of $MoO_3$ nanobelts was dispersed into 50 mL of DI water to form a homogeneous suspension. The as-prepared suspension was filtered through a membrane (pore size of 220 nm). After filtration, the nanopaper formed on the membrane was dried in air for 5 min and then peeled from the filter membrane to obtain a free-standing and semi-transparent $MoO_3$ nanopaper.

The $MoO_3$ nanopaper was cut into ~1.5 mm × 1.5 mm pieces using scissors. A $SiO_2$/Si substrate (area = 10 × 10 $mm^2$, thickness = 0.5 mm) with two platinum electrodes on its top surface (electrode widths of 50 μm and separation of 100 μm) was used as the sensor substrate. To enhance the adhesion between the $MoO_3$ nanopaper and the silicon-wafer substrate, a droplet of DI water (20 μL) was dropped on the substrate using a micro-pipette, and then the $MoO_3$ nanopaper was placed on the substrate. After drying at 60 °C for 20 min, the sensor was annealed at 450 °C for 2 h to remove any residual organic content and to stabilize the sensor at the operation temperature. A schematic image of the $MoO_3$-nanopaper sensor is shown in Fig. 1a.

The crystal structure of the $MoO_3$ nanopaper was investigated using an X-ray diffractometer (Philips X'Pert Pro) with Cu Kα radiation (λ = 1.54184 Å). The morphologies of the sensor were characterized using scanning electron microscopy (SEM, JEOL JSM-6060) and transmission electron microscopy (TEM, Tecnai G20). The reaction between the gas molecules and the sensing materials was analyzed using DRIFT spectra, which were recorded with a VERTEX 70-FTIR spectrometer equipped with a SMART collector and an MCT detector.

The sensors were placed in a quartz tube, and their gas-sensing characteristics were measured at 100–350 °C. A flow-through technique with a constant flow rate of 200 $cm^3$ $min^{-1}$ was used. The gas concentrations were controlled by changing the mixing ratio of the parent gases (TMA, $H_2S$, $NH_3$, $NO_2$, acetone, benzene, ethanol, formaldehyde, toluene, xylene; all 5 ppm in dry synthetic air balance) and dry synthetic air. The interference gases are chosen for the practical applications of sensors in food quality control, environment monitoring and medical diagnosis. A thermocouple was placed near the sample to accurately monitor the sensor temperature. The direct-current two-point probe resistance of the sensor was measured using an electrometer with a computer interface.

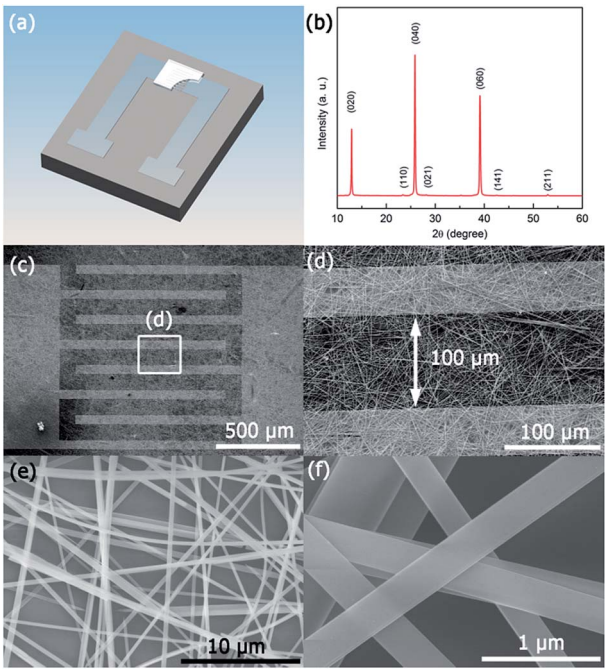


Fig. 1 Schematic figure (a), X-ray diffraction (XRD) pattern (b), and SEM images (c)–(f) of the $MoO_3$-nanopaper gas sensor.

## Results and discussion

According to the XRD pattern shown in Fig. 1b, the nanopaper was identified as orthorhombic $MoO_3$ (JCPDS no. 05-0508) with a highly ordered orientation. SEM images of the $MoO_3$ nanobelt sensor (Fig. 1c–f) confirm that uniform $MoO_3$ nanopapers consisting of highly interconnected $MoO_3$ nanobelts were coated on the electrodes. The $MoO_3$ nanobelts were 200–400 nm wide and 100–200 μm long, indicating that almost every $MoO_3$ nanobelt could bridge two electrodes over the gap (100 μm). The highly interconnected and gas-accessible structures surely promote the gas-sensing reaction and carrier transportation. TEM and SAED images of the $MoO_3$ nanobelts (Fig. 2) reveal that the nanobelts were single-crystalline with interplanar spacings of 0.37 and 0.40 nm along the perpendicular directions, which are consistent with the (002) and (200) *d*-spaces of $MoO_3$.

The responses of the $MoO_3$ nanopaper to 5 ppm $H_2S$ and TMA at 250 and 325 °C are shown in Fig. S1.† The sensor resistance decreased when reducing analyte gas was introduced, which indicates typical n-type sensing. The gas response ($S$) is defined as $R_a/R_g$ for reducing gas; and $-R_g/R_a$ for oxidizing gas, where $R_a$ and $R_g$ are the sensor resistances in air and gas,

Open Access Article. Published on 17 January 2017. Downloaded on 8/17/2025 6:59:34 PM.
This article is licensed under a Creative Commons Attribution 3.0 Unported Licence.

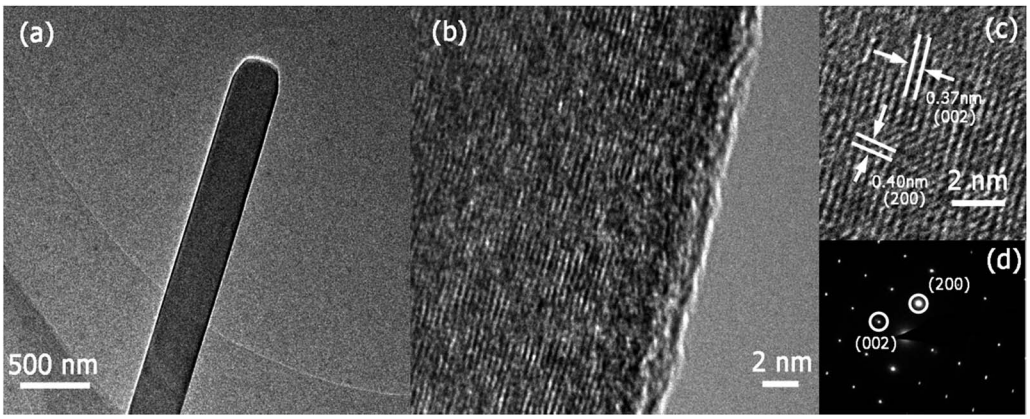


Fig. 2 TEM image (a), high-resolution TEM images (b) and (c), and selected-area electron diffraction (SAED) pattern (d) of $MoO_3$ nanobelts.

respectively. The response and recovery time is defined as the time required to reach 90% variation of the sensor resistance upon exposure to the analyte gas or air. To better illustrate the sensor performance, the gas-sensing characteristics, including the gas response and response and recovery time, are listed in Table S1.†[15,23–25,31,32,34] The $MoO_3$-nanopaper sensor shows relatively rapid gas responses and complete recovery upon exposure to air.

The gas responses of the $MoO_3$-nanopaper sensor to 5 ppm TMA and $H_2S$ were measured at 100–350 °C (Fig. 3). The maximum responses to TMA and $H_2S$ occurred at 325 and 250 °C, respectively. The selectivity of the sensors at different operating temperatures is presented in Fig. 4. At 250 and 325 °C, the $MoO_3$-nanopaper sensor showed good selectivity toward $H_2S$ and TMA, respectively (Fig. 4b and d). The sensor showed a relatively high response to $NH_3$ in the entire range of the sensor temperature (225–325 °C). This demonstrates the potential of the sensor to detect offensive odors. In particular, the comparable and high responses to 5 ppm TMA, $H_2S$, and $NH_3$ at 225 and 275 °C (Fig. 4a and c) indicate that the sensor can be used to detect total irritant gases with unpleasant smells in a selective manner. The all-in-one detection of TMA, $H_2S$, and $NH_3$ can be used in environment monitoring and food quality control.

The response–recovery curves of the $MoO_3$-nanopaper sensor for different gas concentrations are shown in Fig. 5. At 250 °C, the sensor detected 250 ppb $H_2S$ gas with a response of 1.53. At 325 °C, the response to 25 ppb TMA was 4.26, demonstrating that the detection limit was lower. According to the U.S. National Institute for Occupational Safety and Health, the permissible exposure limits of TMA and $H_2S$ are both 10 ppm.[36,37] Although humans can recognize the presence of $H_2S$ at concentrations as low as 10–50 ppb, the human nose cannot quantify the concentration of $H_2S$ and is susceptible to olfactory fatigue.[20] The presence of both gases at a concentration higher than 10 ppm in the ambient atmosphere is known to cause severe irritation to human beings. The presence of TMA and $H_2S$ in human exhaled breath (0.1–0.2 ppm for TMA, 0.1–0.5 ppm for $H_2S$) indicates renal-system imbalance and periodontal disease, respectively.[7,8] Thus, a $MoO_3$-nanopaper sensor with an ultralow gas-detection limit, such as the proposed

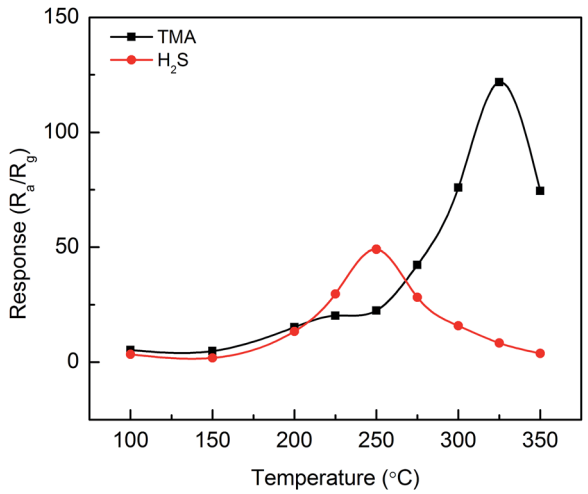


Fig. 3 Responses of the $MoO_3$-nanopaper sensor to 5 ppm TMA and $H_2S$ with respect to the sensing temperature.

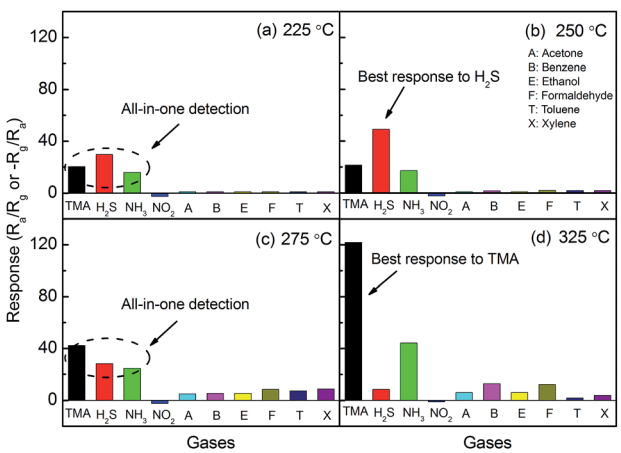


Fig. 4 Selectivity of the $MoO_3$-nanopaper sensor at different operation temperatures: (a) 225 °C, (b) 250 °C, (c) 275 °C, and (d) 325 °C.


This journal is © The Royal Society of Chemistry 2017

Open Access Article. Published on 17 January 2017. Downloaded on 8/17/2025 6:59:34 PM.
This article is licensed under a Creative Commons Attribution 3.0 Unported Licence.

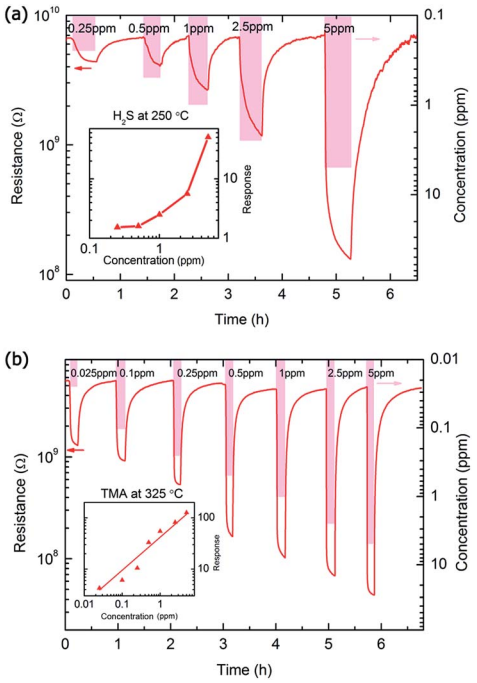


Fig. 5 Response–recovery curves of the $MoO_3$-nanopaper sensor to different $H_2S$ concentrations at 250 °C (a) and different TMA concentrations at 325 °C (b). The insets show the response of the sensor to various gas concentrations.

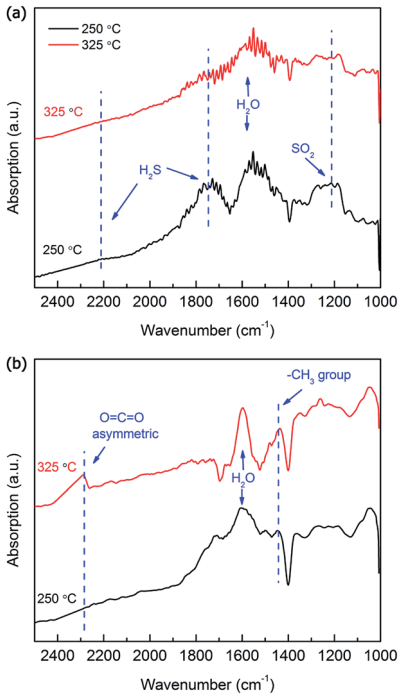


Fig. 6 DRIFT spectra of the $MoO_3$ nanopaper exposed to 50 ppm $H_2S$ (a) and TMA (b) at 250 and 325 °C.

senor, can be used in various applications, including food quality control, environmental monitoring, and medical diagnosis.

The $MoO_3$ sensor showed stable and reversible sensing characteristics upon repetitive exposure to 5 ppm $H_2S$ and TMA, as shown in Fig. S2,† confirming its good stability and reversibility. In general, CuO-loaded n-type semiconductors ($SnO_2$, ZnO, and $WO_3$) show high response and selectivity to $H_2S$ because of the strong chemical interaction between CuO and $H_2S$ and the conversion of semiconducting CuO into metallic CuS.[26,29,38] However, the recovery is sluggish and often incomplete, which is mainly ascribed to the sluggish oxidation of CuS into CuO and/or the deterioration of the sensing surface by sulfur compounds.[39,40] In contrast, $MoO_3$ is known to form non-reactive adsorption compounds such as $MoO_3 \cdot SH_2$ and $MoO_2 \cdot S$ at 100–300 °C, and the material surface can be regenerated by the desorption of sulfur-containing surface species.[41] This shows that $MoO_3$ is a promising material for detecting $H_2S$ in a highly reversible manner. Moreover, acidic $MoO_3$ can enable the detection of other offensive odors with alkaline nature, such as those of TMA and $NH_3$.

The surface reaction of the $MoO_3$ nanopaper was investigated using DRIFT to investigate the gas-sensing mechanism (Fig. 6). Note that gas concentrations 10 times higher (50 ppm $H_2S$ and 50 ppm TMA) were used during the DRIFT measurements in order to observe the interaction between the analyte gas and the sensor surface more clearly. The absorption bands around 2200 and 1750 $cm^{-1}$ are related to the H–S bond; the bands around 1250 $cm^{-1}$ and 1600 $cm^{-1}$ are related to the $SO_2$ and $H_2O$, respectively (Fig. 6a).[42,43] The absorption bands at 1750, 1600, and 1250 $cm^{-1}$ at 250 °C are substantially larger than those at 325 °C. The absorption at 1750 $cm^{-1}$ suggests the active adsorption of $H_2S$, and the absorption at 1600 and 1250 $cm^{-1}$ indicates the promotion of the following gas-sensing reaction to form $H_2O$ and $SO_2$:

$$H_2S + 3O^- \rightarrow H_2O + SO_2 + 3e^- \quad (1)$$

which is consistent with the literature.[31,44]

In Fig. 6b, the absorption band around 1450 $cm^{-1}$ is related to the methyl groups,[45] and that around 2280 $cm^{-1}$ shows the presence of O=C=O bonds, which were due to the asymmetric stretching vibration of $CO_2$ molecules.[46] As explained in Fig. 6a, the absorption band around 1600 $cm^{-1}$ is related to $H_2O$ molecules. The intensities of the three bands are substantially higher at 325 °C than at 250 °C, indicating that an active surface reaction involving the methyl group occurred at 325 °C. The oxidation of TMA into $CO_2$ and $H_2O$ by the reaction with negatively charged surface oxygen can be expressed as a probable sensing reaction:

$$2(CH_3)_3N + 21O^- \rightarrow N_2 + 6CO_2 + 9H_2O + 21e^- \quad (2)$$

This accords with gas-chromatography results from the literature.[34]

The basic mechanism of chemiresistive metal-oxide gas sensing includes the adsorption and desorption of gas molecules, surface reaction, and charge transportation. The $MoO_3$ nanopaper comprised a network of nanobelts that facilitated the adsorption, surface reaction, and desorption of the testing/

Open Access Article. Published on 17 January 2017. Downloaded on 8/17/2025 6:59:34 PM.
This article is licensed under a Creative Commons Attribution 3.0 Unported Licence.

product gases because of the high gas accessibility and large surface-to-volume ratio. When the $MoO_3$ was exposed to air, oxygen molecules absorbed on the surface and formed chemisorbed oxygen species. Thus, a depletion layer was formed, which led to a high sensor resistance. When the $MoO_3$ was exposed to $H_2S$ gas, its high chemical affinity to $H_2S$ promoted the adsorption of $H_2S$ and the gas-sensing reaction (1). DRIFT results clearly show that the $H_2S$-sensing reaction involving the adsorption and oxidation of $H_2S$ was more active at 250 °C (Fig. 6a). When the $MoO_3$ was exposed to TMA, the nitrogen atoms in TMA had a lone pair of electrons that could be donated to form bonds with the Lewis-acid (Mo ion) sites of $MoO_3$. In addition, the methyl group in TMA easily reacted with the negatively charged oxygen on the surface. According to the DRIFT results (Fig. 6b), the gas-sensing reaction (2) was active at 325 °C, confirming that the $MoO_3$ nanopaper had the best response to TMA at 325 °C.

## Conclusions

Free-standing, semi-transparent, flexible $MoO_3$ nanopapers were synthesized by a modified hydrothermal method and filtration. The nanopapers exhibited excellent dual-sensing properties toward $H_2S$ and TMA at different sensing temperatures. The sensor also demonstrated the potential for the all-in-one detection of three representative offensive odors (TMA, $H_2S$, and $NH_3$). The high chemical affinity of $MoO_3$ to $H_2S$ and the regenerative refreshing of the sensor surface are suggested as reasons for the selective, sensitive, and reversible detection of $H_2S$ at 250 °C, while the acid–base interaction between acidic $MoO_3$ and basic TMA was responsible for the selective and sensitive detection of TMA. The mechanism underlying the dual sensing was elucidated using DRIFT analysis. The proposed sensor provides a simple solution to detect various irritant gases in a highly selective manner.

## Acknowledgements

This work was supported by a grant from the National Research Foundation of Korea, which is funded by the Korean government (Ministry of Education, Science, and Technology (MEST): Grant No. 2016R1A2A1A05005331).

## Notes and references

1 W. Zhang and W. Zhang, *Sens. Actuators, B*, 2008, **134**, 403–408.
2 G. Moula, M. Bose and S. Sarkar, *Inorg. Chem.*, 2013, **52**, 5316–5327.
3 R. J. Reiffenstein, W. C. Hulbert and S. H. Roth, *Annu. Rev. Pharmacol.*, 1992, **32**, 109–134.
4 L. Zhang, P. De Schryver, B. De Gusseme, W. De Muynck, N. Boon and W. Verstraete, *Water Res.*, 2008, **42**, 1–12.
5 H. U. Rehman, *Postgrad. Med. J.*, 1999, **75**, 451–452.
6 Y. Sun, X. M. Wang, Y. H. Chen, R. X. Zhu and C. C. Liao, *Chin. Med. J.*, 2013, **126**, 3240–3244.
7 M. A. Bain, R. Faull, G. Fornasini, R. W. Milne and A. M. Evans, *Nephrol., Dial., Transplant.*, 2006, **21**, 1300–1304.
8 A. M. W. T. van den Broek, L. Feenstra and C. de Baat, *J. Dent.*, 2007, **35**, 627–635.
9 I. D. Kim, A. Rothschild and H. L. Tuller, *Acta Mater.*, 2013, **61**, 974–1000.
10 A. Rothschild and H. L. Tuller, *J. Electroceram.*, 2006, **17**, 1005–1012.
11 H. J. Kim and J. H. Lee, *Sens. Actuators, B*, 2014, **192**, 607–627.
12 C. W. Na, H. Woo, I. Kim and J. Lee, *Chem. Commun.*, 2011, **47**, 5148–5150.
13 S. J. Kim, I. S. Hwang, C. W. Na, I. D. Kim, Y. C. Kang and J. H. Lee, *J. Mater. Chem.*, 2011, **21**, 18560–18567.
14 Y. J. Hong, J. W. Yoon, J. H. Lee and Y. C. Kang, *Chem.–Eur. J.*, 2014, **20**, 2737–2741.
15 H. S. Woo, C. H. Kwak, I. D. Kim and J. H. Lee, *J. Mater. Chem. A*, 2014, **2**, 6412–6418.
16 H. M. Jeong, H. J. Kim, P. Rai, J. W. Yoon and J. H. Lee, *Sens. Actuators, B*, 2014, **201**, 482–489.
17 H. Li, Z. Cai, J. Ding and X. Guo, *Sens. Actuators, B*, 2015, **220**, 398–405.
18 K. W. Kim, P. S. Cho, S. J. Kim, J. H. Lee, C. Y. Kang, J. S. Kim and S. J. Yoon, *Sens. Actuators, B*, 2007, **123**, 318–324.
19 D. Li, T. Lei, S. Zhang, X. Shao and C. Xie, *Sens. Actuators, B*, 2015, **221**, 556–563.
20 S. P. Zhang, C. S. Xie, D. W. Zeng, H. Y. Li, Y. Liu and S. Z. Cai, *Sens. Actuators, B*, 2009, **142**, 243–252.
21 P. M. Perillo and D. F. Rodríguez, *J. Alloys Compd.*, 2016, **657**, 765–769.
22 S. Zhu, X. Liu, Z. Chen, C. Liu, C. Feng, J. Gu, Q. Liu and D. Zhang, *J. Mater. Chem.*, 2010, **20**, 9126–9132.
23 Y. H. Cho, Y. C. Kang and J. H. Lee, *Sens. Actuators, B*, 2013, **176**, 971–977.
24 Y. H. Cho, Y. N. Ko, Y. C. Kang, I. Kim and J. Lee, *Sens. Actuators, B*, 2014, **195**, 189–196.
25 X. Chu, S. Zhou, W. Zhang and H. Shui, *Mater. Sci. Eng., B*, 2009, **164**, 65–69.
26 S. J. Kim, C. W. Na, I. S. Hwang and J. H. Lee, *Sens. Actuators, B*, 2012, **168**, 83–89.
27 J. W. Yoon, Y. J. Hong, Y. C. Kang and J. H. Lee, *RSC Adv.*, 2014, **4**, 16067–16074.
28 A. Chowdhuri, V. Gupta, K. Sreenivas, R. Kumar, S. Mozumdar and P. K. Patanjali, *Appl. Phys. Lett.*, 2004, **84**, 1180–1182.
29 N. S. Ramgir, C. P. Goyal, P. K. Sharma, U. K. Goutam, S. Bhattacharya, N. Datta, M. Kaur, A. K. Debnath, D. K. Aswal and S. K. Gupta, *Sens. Actuators, B*, 2013, **188**, 525–532.
30 J. Chen, K. Wang, L. Hartman and W. Zhou, *J. Mater. Chem. C*, 2008, **112**, 16017–16021.
31 Q. Ouyang, L. Li, Q. Wang, Y. Zhang, T. Wang, F. Meng, Y. Chen and P. Gao, *Sens. Actuators, B*, 2012, **169**, 17–25.
32 W. Kim, H. Kim and S. Hong, *J. Nanopart. Res.*, 2010, **12**, 1889–1896.
33 H. Huang, H. Li, X. Wang and X. Guo, *Sens. Actuators, B*, 2017, **238**, 16–23.

 This journal is © The Royal Society of Chemistry 2017

Open Access Article. Published on 17 January 2017. Downloaded on 8/17/2025 6:59:34 PM.
This article is licensed under a Creative Commons Attribution 3.0 Unported Licence.

34 S. Yang, Y. Liu, W. Chen, W. Jin, J. Zhou, H. Zhang and G. S. Zakharova, *Sens. Actuators, B*, 2016, **226**, 478–485.
35 B. Yao, L. Huang, J. Zhang, X. Gao, J. Wu, Y. Cheng, X. Xiao, B. Wang, Y. Li and J. Zhou, *Adv. Mater.*, 2016, **28**, 6353–6358.
36 The National Institute for Occupational Safety and Health (NIOSH), Trimethylamine, Centers for Disease Control and Prevention, Atlanta, GA, USA, 2006, http://www.cdc.gov/niosh/npg/npgd0636.html, accessed on October 2016.
37 The National Institute for Occupational Safety and Health (NIOSH), Hydrogen Sulfide, Centers for Disease Control and Prevention, Atlanta, GA, USA, 2006, http://www.cdc.gov/niosh/idlh/7783064.html, accessed on October 2016.
38 X. Xue, L. Xing, Y. Chen, S. Shi, Y. Wang and T. Wang, *J. Mater. Chem. C*, 2008, **112**, 12157–12160.
39 F. Zhang, A. Zhu, Y. Luo, Y. Tian, J. Yang and Y. Qin, *J. Mater. Chem. C*, 2010, **114**, 19214–19219.
40 C. S. Lee, Y. S. Kim, W. B. Hwang, Y. S. Jung, D. Ragupathy, S. I. Son, D. D. Lee and C. J. Kim, *Sensors*, 2013, **13**, 3889–3901.
41 S. Matsuda, T. Kamo, J. Imahashi and F. Nakajima, *Ind. Eng. Chem. Res.*, 1982, **21**, 18–22.
42 T. J. Toops and M. Crocker, *Appl. Catal., B*, 2008, **82**, 199–207.
43 R. V. Siriwardane and S. Woodruff, *Ind. Eng. Chem. Res.*, 1997, **36**, 5277–5281.
44 S. Bai, C. Chen, R. Luo, A. Chen and D. Li, *Sens. Actuators, B*, 2015, **216**, 113–120.
45 N. Nishino, K. D. Arquero, M. L. Dawson and B. J. Finlayson-Pitts, *Environ. Sci. Technol.*, 2014, **48**, 323–330.
46 J. Ding, H. Li and X. Guo, *Solid State Ionics*, 2015, **272**, 155–159.